

Enhancement of electrical performance of ZnSe thin films via Au nanosandwiching

A.F. QASRAWI^{1,2,*}, MARAM F. TALEB¹

¹Department of Physics, Arab American University, Jenin, Palestine

²Group of physics, Faculty of Engineering, Atilim University, 06836 Ankara, Turkey

In this work, we report the effect of sandwiching of Au nanosheets on the structural and electrical properties of ZnSe thin films. The ZnSe films which are grown by the thermal evaporation technique onto glass and yttrium thin film substrates exhibit lattice deformation accompanied with lattice constant extension, grain size reduction and increased defect density upon Au nanosandwiching. The temperature dependent direct current conductivity analysis has shown that the 70 nm thick Au layers successfully increased the electrical conductivity by three orders of magnitude without causing degeneracy. On the other hand, the alternating current conductivity studies in the frequency domain of 10 MHz to 1800 MHz have shown that the alternating current conduction in ZnSe is dominated by both of quantum mechanical tunneling and correlated barrier hopping of electrons over the energy barriers formed at the grain boundaries. The Au nanosheets are observed to increase the density of localized states near Fermi level and reduce the average hopping energy by ~ 5 times. The conductivity, capacitance, impedance and reflection coefficient spectral analyses have shown that the nanosandwiching of Au between two layers of ZnSe makes the zinc selenide more appropriate for electronic applications and for applications which need microwave cavities.

Keywords: ZnSe; Au; nanosandwiching; conductivity; defects

1. Introduction

Zinc selenide in a thin film and single crystal form is a promising material for technological applications that include bioimaging [1], photovoltaics [2–4] and laser resonators [5]. Recently, highly blue fluorescent cysteamine coated ZnSe quantum dots in aqueous medium have been prepared at near physiological pH by a fast precipitation process followed by hydrothermal growth technique. This type of highly fluorescent quantum dots has been reported to be suitable as new low toxic and promising platform for biolabeling purposes [1]. In addition, heterojunctions which comprise p-type ZnSe nanoribbons and n-type Si nanowires have been employed as p-n nanoheterojunction which exhibited photovoltaic behavior, with power conversion efficiency of $\sim 3\%$ [2]. Furthermore, room temperature investigations of kinetics of Fe:Cr:ZnSe under laser excitation of a wavelength of 1560 nm have shown

that the energy transfer between Fe and Cr centers is as fast as 290 ns, which makes this material attractive for the use as a pumping mechanism for Fe lasing [3].

Various techniques have been employed to enhance the electrical performance of ZnSe to make it more appropriate for the electrical and optoelectronic applications. For example, annealing of ZnSe thin films under vacuum pressure of 10^{-1} Pa at 473 K for one hour increased the grain size from 15 nm to 18 nm and increased the electrical conductivity from $1.76 \times 10^{-6} (\Omega \cdot \text{cm})^{-1}$ to $3.11 \times 10^{-6} (\Omega \cdot \text{cm})^{-1}$. It also shifted the conductivity activation energy from 0.75 to 0.97 eV [4]. In addition, preparing ZnSe thin films at different substrate temperatures in the range of 298 K to 373 K has been studied too. An increase in dark conductivity from $2.19 \times 10^{-8} (\Omega \cdot \text{cm})^{-1}$ to $6.59 \times 10^{-8} (\Omega \cdot \text{cm})^{-1}$ was reported in [5]. The photoconductivity also increased by two orders of magnitude as the substrate temperature increased from 298 K to 373 K.

*E-mail: atef.qasrawi@atilim.edu.tr

As an alternative technique, we have tried to improve the electrical performance of ZnSe via nanosandwiching technique. Particularly, a nanosheet of Au was inserted between two layers of ZnSe for the purpose of increasing the electrical conductivity of ZnSe. Both the direct current (DC) and alternating current (AC) conductivities were studied and analyzed. While the DC conductivity was studied as a function of temperature, the AC conductivity was studied in the frequency domain of 10 MHz to 1800 MHz. The dominant current conduction mechanisms and the electrical conductivity parameters were also investigated in terms of technological applications.

2. Experimental

Zinc selenide layers of thicknesses of 500 nm were prepared by the physical evaporation technique onto glass substrates from high purity ZnSe powders (Alpha Aeser 99.99 %) in a thermal vacuum system under a vacuum pressure of 10^{-3} Pa. Some of the produced ZnSe layers were employed as substrates to deposit layers of pure (99.97 %) Au nanosheets (70 nm). The produced ZnSe/Au films were then used as substrates to deposit another ZnSe (500 nm) layers so that nanosandwiched structure was created. The thickness was controlled by an in situ STM-2 thickness monitor connected to a quartz crystal inside a vacuum chamber. CuK α radiation Miniflex 600 X-ray unit was used to explore the structural changes associated with the nanosandwiching process. The direct current measurements were carried out in a high temperature cryostat and the room temperature alternating current measurements were realized with the help of Agilent 4291B 10-1800 MHz impedance analyzer.

3. Results and discussion

For the purpose of enhancing the electrical properties of ZnSe thin films, an Au nanosheet of a thickness of 70 nm was inserted between two 500 nm thick ZnSe films. The thickness of Au represents only 7 % of the total thickness of the studied films. The resulting X-ray

diffraction patterns for two Au sandwiched stacked layers of ZnSe/Au/ZnSe (ZAZ) and unsandwiched ZnSe/ZnSe (ZZ) are shown in Fig. 1. The figure displays polycrystalline nature of the films with two intensive peaks centered at diffraction angles (2θ) of 28.10° and 25.4° . The insertion of Au nanosheet shifts the peaks positions to 28.0° and 25.3° . The shift in the major peak center is also shown in the inset of Fig. 1. The shift toward lower diffraction angles is an indication of lattice extension due to deformation. The calculated lattice parameters for the hexagonal ZnSe thin films before the insertion of Au nanosheet was found to be $a = 4.051$ and $c = 6.354$ Å. These values are consistent with literature data [6]. The insertion of Au changed the lattice parameters to $a = 4.066$ and $c = 6.376$ Å. Such extension in the lattice parameters is accompanied with strain ($E = (a_{ZAZ} - a_{ZZ}) / a_{ZZ}$), of the values 3.70×10^{-3} and 3.46×10^{-3} along the a and c axis, respectively. Such values of strain lead to high value of defect density ($\delta = \frac{15c}{aD}$ where D is grain size). The grain size and defect density obtained from the full wave at half maximum of the major peak which is oriented along the (0 0 2) direction are found to be 29 nm and 4.33×10^{11} lines/cm 2 and 21 nm and 7.69×10^{11} lines/cm 2 , before and after the insertion of Au nanosheet, respectively.

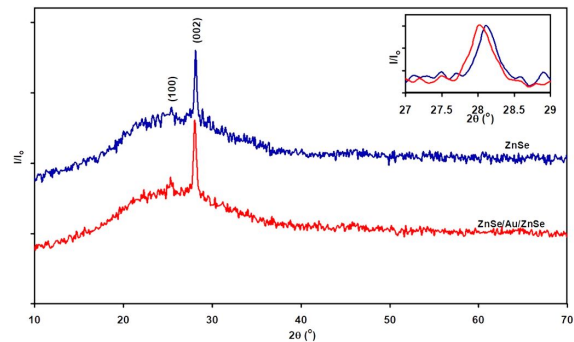


Fig. 1. X-ray diffraction patterns for ZnSe/ZnSe, and ZnSe/Au/ZnSe films.

The selection of this Au thickness is related to the fact that the dislocations at the interface are inevitable due to the physical mismatch of terminating bonds at the interface, which can be eliminated by reducing the thickness. The lattice mismatch is

defined as $\Delta = |a_e - a_s|/a_e$ (a_e : epitaxial, a_s : substrate) and the critical thickness is $t_c = a_e/(2\Delta)$. Taking into account that the lattice constant of cubic Au is 4.0782 Å, the lattice mismatch between the Au nanosheets and ZnSe film is 6.67×10^{-3} along the a axis and 0.558 along the c axis. This leads to critical thicknesses of values of 30.57 nm along the a axis and 0.365 nm along the c axis. For this reason, sufficiently thick layers of Au sheet is used to guarantee the uniform and continuous distribution of gold over ZnSe. One reason beyond the extension in the lattice parameters which caused high values of strain and larger defect density upon nanosandwiching of gold between two layers of ZnSe could be the increase in the adjacent planes distance with the inclusion of Au atoms as observed at Au/ZnO interfaces [7]. The inclusion of Au atoms into the structure of ZnO shifted the diffraction angles toward lower angles owing to the larger ionic radius of Au^{+3} (82 pm) compared to that of Zn^{+2} (74 pm). For ZnO thin films, the higher the Au content, the higher the strain, the smaller the grain size and the higher the defect density [7].

In order to reveal information about the effect of Au nanosheets on direct current (DC) conduction of the ZnSe thin films, the electrical conductivity was measured in the temperature range of 310 K to 450 K. The near room temperature electrical conductivity increased from 1.62×10^{-6} to $3.25 \times 10^{-3} (\Omega \cdot \text{cm})^{-1}$. An increase by three orders of magnitude has been achieved by the Au nanosandwiching. On the other hand, the Arrhenius plots which are shown in Fig. 2a and Fig. 2b for the ZnSe and ZnSe/Au/ZnSe thin films, respectively, reveal linear slopes of the $\ln(\sigma)$ vs. T^{-1} . The calculated conductivity activation energies (E_σ) before and after the nanosandwiching process have been found to be 0.822 eV and 0.942 eV, respectively. These values of activation energies are close to those reported for the as-grown and annealed ZnSe thin films being 0.75 eV and as 0.97 eV, respectively [4]. Recalling that the hot probe tests have shown that both samples exhibit n-type conductivity, the extension of the lattice that resulted from the Au nanosandwiching has been accompanied with the formation of deep donor levels in the band gap of ZnSe. Assuming that the Fermi

level is located at the midpoint between the donor level and the bottom of the conduction band, and remembering that the electron affinity of ZnSe is 4.09 eV [8], then the work function of ZZ and ZAZ samples turns out to be 4.501 eV and 4.561 eV, respectively. Comparing the Au nanosandwiched ZnSe films with those nanosandwiched with indium nanosheets (75 nm) [9], it can be deduced that the indium forms shallow donor levels and the Au forms deep donors. In addition, various doping agents including Ga, Cl, F and indium have been reported to result in shallow doping level of ~ 29 meV [9]. While In^{+3} ($5s^2 4d^{10} 5p^1$) whose ionic radii is 92 pm [10], which is also larger than that of Zn, contributes three valence electrons to the energy band structure of ZnSe, Au ($6s^1 4f^{14} 5d^{10}$) contributes five valence electrons to the band structure of ZnSe. Since the electronic configuration of Zn^{+2} is $4s^2 3d^{10}$ and it shares only two valence electrons, the Au nanosheets provide the feature of having more valence electrons. In addition, as the 4f and 5d states are at higher energy levels than those of 3d or 4d states, an orbital overlapping between Au and Zn or Se atomic orbitals occurs. Such electronic structure explains the reason for the increase in the electrical conductivity via Au nanosandwiching. It is also worth of consideration that while the indium nanosandwiching reveals degenerate levels in ZnSe making it degenerate semiconductor, Au keeps the material nondegenerate.

It is also interesting to assume that the conductivity activation energy may be connected with the grains and grain boundaries. It is well known that polycrystalline thin films exhibit potential barriers ($q\phi_b$) at the grain boundaries [11, 12]. For a film composed of large grains which are very close to each other, the conductivity of the grains is much higher than the conductivity of grain boundaries. Since the conductivity is defined by:

$$\begin{aligned} \sigma &= \sigma_o \exp\left(-\frac{E_\sigma}{kT}\right) \\ &= ne\mu = n_o\mu_o \exp\left(-\frac{E_d + q\phi_b}{kT}\right) \end{aligned} \quad (1)$$

with n_o , μ_o and σ_o being the pre-exponential factors for the free charge carriers (n) and mobility

(μ) while $E_\sigma = E_d + q\phi_b$ [11, 12]. For this reason, assuming that the donor level is moderately influenced by the Au participation as no atomic Au substitution can take place in the vacant sites of Zn, the deeper activation energy of Au nanosandwiched ZnSe can be assigned to the decrease in the grain size that, in turn, causes an increase in the number of grain boundaries and increase in barrier height at the grain boundaries.

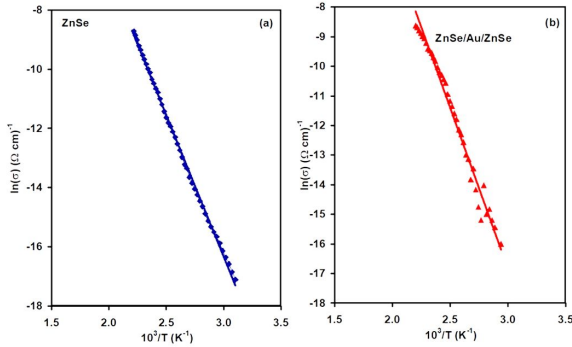


Fig. 2. Arrhenius plots of DC conductivity for (a) ZnSe/ZnSe and (b) ZnSe/Au/ZnSe sandwiched films.

In order to explore the effect of Au nanosandwiched layer on the alternating current (AC) conduction mechanism of ZnSe thin films, the sandwiched and pure layers of ZnSe were deposited onto an ohmic Yb substrate ($q\phi_b = 2.51$ eV) and recoated with Au Schottky point contact ($q\phi_b = 5.34$ eV) on the top layer of the ZZ and ZAZ samples. The AC conductivity ($\sigma_{ac}(\omega)$) spectra which have been recorded in the microwave frequency domain of 10 MHz to 1800 MHz are displayed in Fig. 3. As can be seen from the figure, the conductivity increases with increasing frequency up to 210 MHz, exhibiting a maximum at 210 MHz. The AC conductivity value of the ZAZ samples is three times higher than that of ZZ samples indicating that the Au nanosandwiching has also enhanced the AC conductivity of the ZnSe thin films.

The trends of variation of frequency dependent conductivity indicate the domination of more than one transport mechanism in the samples under study. For this reason, the conductivity was modeled assuming domination of quantum mechanical

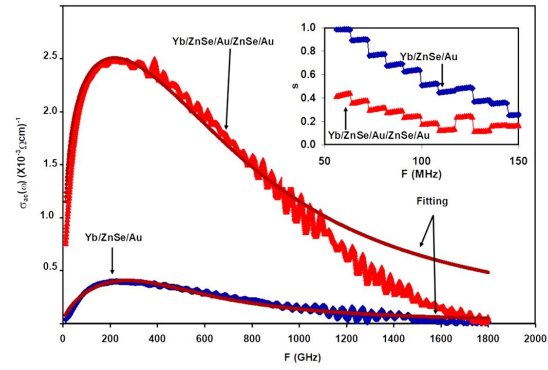


Fig. 3. AC conductivity spectra for ZnSe/ZnSe and ZnSe/Au/ZnSe sandwiched films. The inset shows the s parameter variation with frequency.

tunneling (QMT) and correlated barriers hopping (CBH) conduction mechanisms. The frequency dependence of the AC conductivity is expressed by the equation:

$$\sigma_{ac}(\omega) = A\omega^s \quad (2)$$

Here, $\omega = 2\pi f$ is the angular frequency of the applied AC field, A and the frequency exponent s ($0 \leq s \leq 1$) are parameters. The constant A determines the strength of polarization and s is the Jonscher coefficient representing the amount of interactions between the mobile ions and the lattice around them [13–15]. While the quantum mechanical tunneling (QMT) model assumes tunneling of charge carriers between two localized states near the Fermi level, the correlated barrier hopping mechanism assumes that the charge carrier hops from site to site over the potential barrier [13] at the grain boundaries. s value being 1.0 appears when the distribution of relaxation time ($N(\tau)$) is inversely proportional to τ . Under these conditions, the relaxation time is given by the equation:

$$\tau = \tau_o \exp(2\alpha R) \quad (3)$$

with R being intersite separation and α ($\alpha^{-1} = 10 \text{ \AA}$) is a spatial decay parameter for the wave function employed to represent the localized state at each site. The AC conductivity for an electron undergoing quantum mechanical tunneling can be presented by the equation [14]:

$$\sigma_T(w) = \frac{\pi^4}{24} e^2 kT \alpha^{-1} (N(E_F))^2 w R_w^4 \quad (4)$$

Here, $N(E_F)$ is the density of localized states near the Fermi level and $R_w = \ln(1/(w\tau_0))/(2\alpha)$ is the hopping distance at a particular frequency (w). In the quantum mechanical tunneling model $s = 1 - \frac{4}{\ln\left(\frac{1}{(w\tau_0)}\right)}$. The domination of tunneling process should be valid as s appreciably decreases with increasing frequency at a particular temperature. By finding the derivative $s = d\ln(\sigma(w))/d\ln(w)$ which is illustrated in the inset of Fig. 3, we observed that the domination of the quantum mechanical model is in the range of ~ 60 MHz to 150 MHz.

On the other hand, the correlated barrier hopping conduction (CBH) indicates that $\tau = \tau_0 \exp(W_h/kT)$ with W_h being the hopping barrier height. For such case, the AC conductivity increases with frequency as long as the frequency of the propagating signal is less than the charge carrier jump frequency [14–16]. The AC conductivity in this case is given by the relation:

$$\sigma_{CBH}(w) = \sigma_H(w) + (\sigma_L(w) - \sigma_H(w))/(1 + w^2\tau^2) \quad (5)$$

Here, the subscript symbols H and L mean high and low frequency saturation conductivities, respectively. Applying these theories to our case, it was possible to reproduce the AC conductivity assuming the domination of two conduction mechanisms in the heterojunction device presented by the relation:

$$\frac{1}{\sigma(w)} = \frac{1}{\sigma_T} + \frac{1}{\sigma_{CBH}} \quad (6)$$

The theoretically computed AC conductivity is represented by the brown colored curves in Fig. 3. The good consistency between the experimental and theoretical data was achieved by substituting the fitting parameters which are shown in Table 1. The most reasonable reason for the domination of tunneling mechanism is the ability of charge carriers to find paths through ultrathin regions at the Au/ZnSe interface to reach the conduction band of ZnSe (flowing back from metal to semiconductor). These thin regions could have resulted from the rough surface of ZnSe [17, 18]. On the other hand, the presence of correlated barrier hopping is

attributed to the hopping of electrons between defect centers over the potential barriers separating them and/or barriers separating the grains.

In accordance with the data of Table 1, the insertion of the Au nanosheets between two layers of ZnSe reduced the average hopping energy from 0.396 to 0.080 eV and increased the density of localized states near the Fermi level from 1.1×10^{19} ($\text{eV}^{-1} \cdot \text{cm}^{-3}$) to 5.00×10^{19} ($\text{eV}^{-1} \cdot \text{cm}^{-3}$). This increase may be assigned to the increased defect density from 4.33×10^{11} lines/cm² to 7.69×10^{11} lines/cm² caused by Au nanosandwiching. In addition, the increase in the stacking faults could also be a reason for the observed increase in $N(E_F)$. While the increase in the values of the $\sigma_{ac}(H)$ and $\sigma_{ac}(L)$ can be assigned to the orbital energy bands overlapping, the increase in the relaxation time is assigned to the structural modifications.

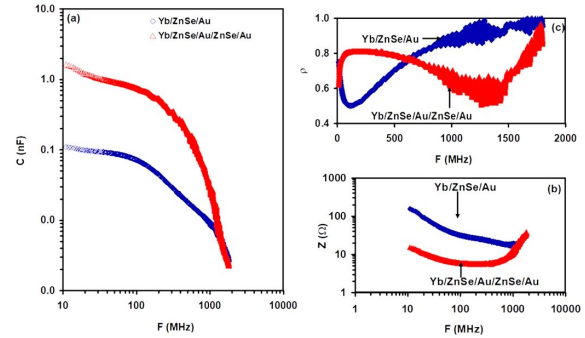


Fig. 4. (a) capacitance, (b) impedance and (c) reflection spectra for ZnSe/ZnSe and ZnSe/Au/ZnSe sandwiched films.

From practical point of view, the effect of Au nanosheets on the capacitance and impedance spectra is shown in Fig. 4a and Fig. 4b, respectively. As seen, the capacitance (C) spectra follow the same shape variation before and after the nanosandwiching of Au. However, the presence of Au inside the ZnSe layers increased the capacitance value (Fig. 4a) by at least one order of magnitude. The decrease in the capacitance with increasing frequency in the frequency domain of 10 MHz to 1300 MHz is faster for the ZAZ samples compared to the unsandwiched ones. In addition, the impedance spectra which are displayed

Table 1. AC conductivity fitting parameters for the quantum mechanical tunneling (QMT) and correlated barrier hopping (CBH) conduction mechanism for Yb/ZnSe/Au and Yb/ZnSe/Au/ZnSe/Au sandwiched films at 300 K.

	Yb/ZnSe/Au	Yb/ZnSe/Au/ZnSe/Au
W_h [eV]	0.396	0.080
$N(E_f) \times 10^{19}$ [eV ⁻¹ ·cm ⁻³]	1.10	5.00
$\tau \times 10^{-9}$ [s]	5.00	1.30
$\sigma_{ac}(H) \times 10^{-3}$ [Ω ·cm ⁻¹]	10.0	60.0
$\sigma_{ac}(L) \times 10^{-2}$ [Ω ·cm ⁻¹]	40.0	36.0

in Fig. 4b show a decreasing trend of variation down to 1300 MHz, where the impedance starts to increase with increasing frequency. The presence of Au nanosheets lowers the magnitude of the impedance significantly. As the frequency exceeds 1300 MHz, the C and Z spectra of both the ZZ and ZAZ samples display the same value and the same trend of variation. On the other hand, the reflection coefficient (ρ) spectrum, which has been calculated by the previously described methods [19] and is illustrated in Fig. 4c indicates distinguished difference between the behavior of ρ before and after the nanosandwiching process. Particularly, while the ZZ sample shows band pass filter features with notch frequency of 130 MHz, the ZAZ sample displays a notch frequency near 1300 MHz. Such features of the produced films indicate the applicability of ZAZ films in microwave technology as band pass filters. The features of the currently reported device are much different from those obtained by the indium nanosandwiching between two layers of ZnSe [9]. Namely, the ZnSe/In/ZnSe samples display a negative capacitance spectra with continuously increasing impedance values with increasing frequency. The notch frequency of the ZIZ filters is 1.0 GHz. Thus, the Au nanosandwiching makes the ZnSe microwave filters response to higher frequency domains.

4. Conclusions

In this study, we succeeded in enhancing the electrical properties of ZnSe thin films via gold nanosandwiching between two layers of ZnSe. A thin layer of Au was sufficient to increase the electrical conductivity by three orders of magnitude

through engineering the barrier height at the grain boundaries. The Au nanosandwiching was also able to increase the alternating current conductivity at high and low frequencies by at least one order of magnitude. The investigations on the current transport mechanisms have shown that the alternating current conduction mechanism is dominated by the quantum mechanical tunneling and correlated barriers hopping below and above 150 MHz, respectively. The Au nanosandwiching decreased both the hopping energies and scattering time and increased the density of localized states near the Fermi level. The engineering of the electrical parameters presented by the conductivity, capacitance, impedance and reflection coefficient spectra in the frequency domain of 10 MHz to 1800 MHz, via Au nanosandwiching, make the ZnSe thin films more suitable for electronic applications which require moderate values of electrical conductivity and applications that require microwave resonators.

Acknowledgements

This project was funded by the Deanship of Scientific Research (DSR) at the Arab American University, Palestine (AAUP). The authors, therefore, acknowledge with thanks the DSR and the AAUP technical and financial support for the 2018-2019 Cycle I project.

References

- [1] MOURA I.M., CABRAL FILHO P.E., SEABRA M.A., PEREIRA G., PEREIRA G.A., FONTES A., SANTOS B.S., *J. Lumin.*, 201 (2018), 284.
- [2] ZHANG X., WU D., HU D., TANG Z., GENG H., TIAN J., JIE J., *Sol. Energ. Mat. Sol. C.*, 176 (2018), 411.
- [3] CARLSON T., GAFAROV O., FEDOROV V., MIROV S., *Osa. Trends Opt. Photo.*, (2018), AW3A-7. <https://doi.org/10.1364/ASSL.2018.AW3A.7>

- [4] SHIKHA D., MEHTA V., SHARMA J., CHAUHAN R.P., *J. Mater. Sci.-Mater. El.*, 29 (2018), 1.
- [5] SHARMA J., SINGH H., SINGH T., THAKUR A., *J. Mater. Sci.-Mater. El.*, 29 (2018), 5688.
- [6] MENDIL R., AYADI Z.B., VÁZQUEZ-VÁZQUEZ C., LÓPEZ-QUINTELA M.A., DJESSAS K., *J. Mater. Sci.-Mater. El.*, 29 (2018), 1.
- [7] ABAD S.N.K., MOGHADDAM J., MOZAMMEL M., MOSTAFAEI A., CHMIELUS M., *J. Alloy. Compd.*, 777 (2019), 1386.
- [8] WONGCHAROEN N., GAEWANG T., *In Key Eng. Mater.*, 775 (2018), 246.
- [9] GARNI S., *Chalcogenide Lett.*, 14 (2017), 545.
- [10] LEE H.C., LEE J.A., LEE J.H., HEO Y.W., KIM J.J., *Ceram. Int.*, 43 (2017), 11792.
- [11] QASRAWI A.F., PARLAK M., ERCELEBI C. GÜNAL I., *J. Mater. Sci.-Mater. El.*, 12 (2001), 473.
- [12] WANG S., HUI S., PENG K., BAILEY T.P., ZHOU X., TANG X., UHER C., *J. Mater. Chem. C*, 5 (2017), 10191.
- [13] SHARMA S., SINGH M.M., MANDAL K.D., *Ceram. Trans.*, 252 (2015), 95.
- [14] KHUSAYFAN N.M., QASRAWI A.F., KHANFAR H.K., *Mater. Res. Express*, 5 (2018), 026303.
- [15] GHOSH A., *Phys. Rev. B*, 41 (1990), 1479.
- [16] FURLAN J., SKUBIC I., SMOLE F., POPOVIC P., TOPIC M., *J. Appl. Phys.*, 80 (1996), 3854.
- [17] KHUSAYFAN N.M., QASRAWI A.F., KHANFAR H.K., *Mater. Sci. Semicond. Proces.*, 64 (2017), 63.
- [18] YUDAR H.H., PAT S., KORKMAZ Ş., ÖZEN S., ŞENAY V., *J. Mater. Sci.-Mater. El.*, 28 (2017), 2833.
- [19] KHANFAR H.K., QASRAWI A.F., SHEHADA S.R., *J. Electron. Mater.*, 48 (2018), 244.

Received 2018-12-30
Accepted 2019-04-23